

Hybrid deep learning-based strategy for the hepatocellular carcinoma cancer grade classification of H&E stained liver histopathology images

Ajinkya Deshpande, Deep Gupta *Senior Member, IEEE*, Ankit Bhurane *Member, IEEE*, Nisha Meshram, Sneha Singh *Member, IEEE*, Petia Ivanova Radeva

Abstract—Hepatocellular carcinoma (HCC) is a common type of liver cancer whose early-stage diagnosis is a common challenge, mainly due to the manual assessment of hematoxylin and eosin-stained whole slide images, which is a time-consuming process and may lead to variability in decision-making. For accurate detection of HCC, we propose a hybrid deep learning-based architecture that uses transfer learning to extract the features from pre-trained convolutional neural network (CNN) models and a classifier made up of a sequence of fully connected layers. This study uses a publicly available The Cancer Genome Atlas Hepatocellular Carcinoma (TCGA-LIHC) [1] database (n=491) for model development and proprietary database of Kasturba Gandhi Medical College (KMC), India [2] for validation. The pre-processing step involves patch extraction, colour normalization, and augmentation that results in 3920 patches for the TCGA dataset. The developed hybrid deep neural network consisting of a CNN-based pre-trained feature extractor and a customized artificial neural network-based classifier is trained using five-fold cross-validation. For this study, eight different state-of-the-art models are trained and tested as feature extractors for the proposed hybrid model.

The proposed hybrid model with ResNet50-based feature extractor provided the sensitivity, specificity, F1-score, accuracy, and AUC of 100.00%, 100.00%, 100.00%, 100.00%, and 1.00, respectively on the TCGA database. On the KMC database, EfficientNetb3 resulted in the optimal choice of the feature extractor giving sensitivity, specificity, F1-score, accuracy, and AUC of 96.97 ± 0.83 , 98.85 ± 0.24 , 96.71 ± 0.66 , 96.71 ± 0.66 , and 0.99 ± 0.01 , respectively. The proposed hybrid models showed improvement in accuracy of 2% and 4% over the pre-trained models in TCGA-LIHC and KMC databases.

Index Terms—HCC classification, ResNet, EfficientNet, VGG16, DenseNet, Deep learning, transfer learning, fine-tuning.

I. INTRODUCTION

GLOBALLY, over 700,000 people die every year from liver cancer, making it the third most common cause of cancer-related death [3] [4]. The hepatocellular carcinoma (HCC) is the most common type of liver cancer accounting

A. Deshpande, D. Gupta and A. Bhurane are with the Department of Electronics and Communication Engineering, Visvesvaraya National Institute of Technology, Nagpur, MH, India (e-mail: 39ajinkya@gmail.com, deepgupta@ece.vnit.ac.in, ankitbhurane@ece.vnit.ac.in)

N. Meshram is with the Department of Pathology, AIIMS Nagpur, MH, India (e-mail: drnisha@aiimsnagpur.edu.in.)

Sneha Singh is with the School of Computing & Electrical Engineering, the Indian Institute of Technology Mandi, India (e-mail:sneha@iitmandi.ac.in)

P. Radeva is with the Department of Mathematics and Informatics, Universitat de Barcelona, 08007, and Computer Vision Center, Cerdanyola 08007 (Barcelona), Spain (e-mail:petia.ivanova@ub.edu).

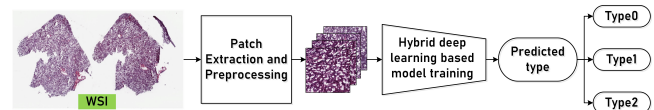


Figure 1. Block diagram showing overall workflow of the experimentation

for almost 80% of all the primary liver cancer cases [5], [6]. A major spread of the HCC has been observed in Asian and African countries. Pathologists consider histopathology imaging as a gold standard to identify HCC [7]. However, due to the diversity in tumor shape, tissue sizes and staining procedure, manual assessment of such histopathology images is often a challenging and error-prone task [8] [9] [10].

With the advancements in artificial intelligence (AI), the landscape of medical diagnosis has completely changed, and it has helped over the years the medical community in providing patients with accurate and inexpensive computer-aided diagnostic solutions for the betterment of their health [11]. In the domain of liver cancer detection, the AI-based convolutional neural network (CNN) algorithms have contributed to a great extent in the prediction of cancer types [6] [2] [12] [13] [7] replacing traditional techniques such as SVM [14]. In the past decade, several CNN-based architectures have been proposed that either focus on deepening the network such as AlexNet [15] and VGG [16] or to overcome the vanishing gradient issue by adding the residual connections ResNet [17] architectures and DenseNet [18] or applying compound scaling methodology that demonstrates dependency on width, depth and resolution of CNN through EfficientNet architectures [19]. These models have been used as state-of-the-art for a long time and possess special features. Most of the recent studies used such CNN architecture as their backbone models. Unlike the conventional machine learning (ML)-based algorithms, the CNNs do not require handcrafted features for training. The architecture of CNN is responsible for both feature extraction and classification eventually achieving better performance than traditional methods [20] [21] and providing an end-to-end solution. This is the primary reason for their popularity in performing medical image classification [22].

Recently, Sun et al. [12] used a ResNet50 to perform the liver cancer classification using global image-based labels. The authors proposed patch extraction and feature selection mechanisms. Chen et al. [13] used the InceptionV3 to perform the patch-level liver cancer classification on the TCGA dataset.

Atresh et al. [2] proposed a new LiverNet architecture, which consisted of a convolutional block attention module block (CBAM), atrous convolution spatial pyramid pooling blocks, and hypercolumn technique, which reduces model parameters as well as makes the model more robust and precise. The authors claimed the overall liver cancer detection accuracy of 97.72%. In another study, Chen et al. [7] studied the performance of ResNet50, ResNet50_CBAM, SENet, and SKNet on purely, moderately and well-differentiated histopathology images. SENet and ResNet50 were found to be the best-performing models on poorly and well-differentiated types, respectively. Another study [23] proposes prior segmentation for better classification accuracies. Luo et al. [24] by employing a deformable convolution guided attention block and deep adaptive feature fusion, proposed DCA-DAFFNet for laryngeal tumor grading and achieves accuracy of 90.78%. Similarly, few more recent studies use the CNN-based algorithms for histopathology image classification [25] [26] [20] [27].

All these studies used the diverse CNN-based architecture for the liver cancer classification. Most of these studies also use two most important concepts i.e. transfer-learning and fine-tuning. In transfer learning, the model trained on the diversified and huge database with multiple classes is used to train on a small dataset with a limited number of classes [28] [29] [30] [31]. Similarly, in fine-tuning, selective top layers of feature extractor along with the classifier are made trainable [25] [32] [33] [26] [34]. Recent study by Talo et al. [30] suggest that if some of the top layers of the feature extractor are kept trainable along with the classifier, then better classification accuracy can be achieved.

Motivated by the concept of transfer learning and fine-tuning, and observing that keeping selective top feature extractor layers along with classifier trainable can boost overall classification performance [25], we developed a hybrid CNN-based architecture for liver cancer classification. We hypothesized that the proposed hybrid deep learning-based architecture may perform better than the individual pre-trained models. The salient contributions are listed as follows:

- 1) Fine-tuning powered model is designed to address the issues in cross-domain learning. In the proposed work, the effect of transferring the learnings to the medical domain and tuning the model to a certain depth for new characterization is studied.
- 2) Classifier designed with fully connected layers with gradual feature reduction to ensure proper mapping to the output label space. This also helps to develop an optimum end-to-end solution for histopathological image classification.
- 3) This study also demonstrates the importance of proper image pre-processing and training methodology for better loss convergence, achieving optimum results and developing the robust model.

The rest of the paper is organized as follows. Section 2 discusses the details of the dataset, preprocessing, a proposed model architecture, performance metrics and training methodology. Section 3 describes the experimental details with results validation along with a detailed comparative study. In Section

4, a detailed discussion on the experimental results obtained, followed by the conclusion in Section 5. The overall workflow for the experimentation is shown in Fig. 1

II. METHODS

A. Datasets and Pre-processing

This study uses a publicly available cancer genome atlas program liver hepatocellular carcinoma (TCGA-LIHC) database of 491 whole slide images [1] to train the proposed hybrid deep learning-based model. The 491 slides were divided into three types of liver HCC tumor namely solid tissue normal as type 0, primary tumor as type 1, and recurrent tumor as type 2. There were 89 solid tissue normal slides, 399 primary tumor slides, and 3 recurrent tumor slides in total. In a deep learning-based approach for classification, directly feeding the whole slide images of very large dimensions to CNN is nearly impractical as it increases computations and model parameters by a large amount. Downsampling or reshaping the histopathology images to lower dimensions leads to severe information loss. Therefore, we follow a patch-based approach [12], where each WSI slide is tiled into patches of size 1024×1024 . While performing the patch extraction, we also intended to maintain sufficient visibility of tissues in the patches. This was ensured by maintaining the mean intensity value of 200 and the standard deviation of 60. An empirical selection process is performed to maintain the clear visualization of tissues in the patches and to reduce the class imbalance in the database. Finally, 813, 893, and 680 valid patches of type 0, type 1 and type 2, respectively are considered to develop the proposed hybrid deep learning-based model.

The color normalization is another important step in the pre-processing of histology images because the variation of staining intensity of hematoxylin and eosin used for staining purposes in the histology images by the pathologist and may vary according to the practitioner and physical conditions. Thus, the color variations can significantly impact the model training because models are colour-sensitive. In the proposed study, we used the color normalization technique proposed by Macenko et al. [35] which presents an algorithm that finds the correct stain vectors for the image after converting image pixels to optical density space automatically and then performs colour deconvolution.

Deep learning models require a diverse and large dataset to build robust and flexible networks. Augmentation is a technique which generates variants of existing data ultimately increasing the dataset. This makes data augmentation an important step in preprocessing. Over the normalized patches, we applied random vertical and horizontal flips and obtained 1220, 1340, and 1360 patches of type 0, type 1, and type 2 respectively. The complete pre-processing stage is depicted in Fig. 2.

This study also uses another cancer database of liver HCC collected from Kasturba Gandhi Medical College, India [2]. The KMC database had four types of liver HCC tumors such as type 0, type 1, type 2, and type 3 having 719, 799, 776, 711 image patches, respectively, each of size $224 \times 224 \times 3$.

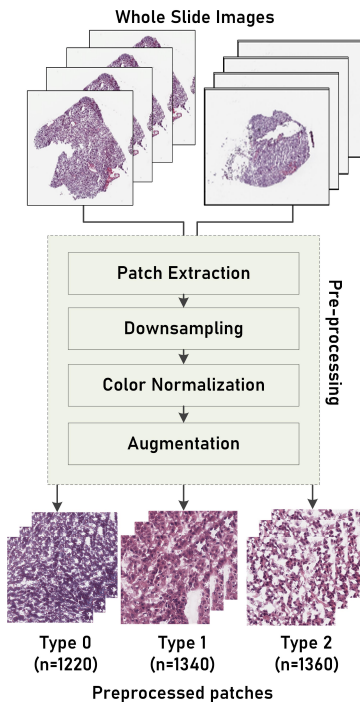


Figure 2. TCGA-LIHC liver HCC database [1]. This diagram describes the workflow overall TCGA dataset preparation which involves patch extraction from whole slide images, then downsampling to balance the dataset, and augmentation. After data preprocessing the number of images obtained are mentioned in the table.

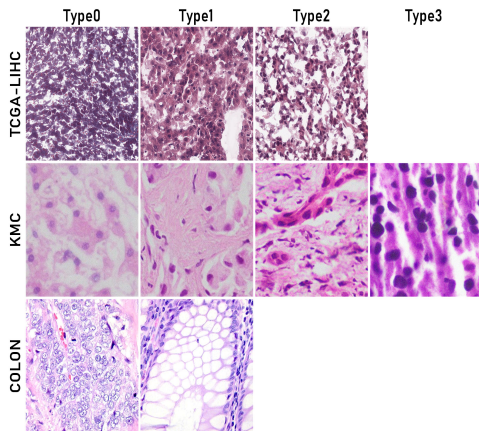


Figure 3. TCGA-LIHC, KMC and COLON datasets are comprised of 3, 4 and 2 types respectively. This figure shows demo patches available in the respective dataset.

The received KMC database [2], was originally pre-processed and, therefore, only the augmentation step is performed during the training of the proposed model. Moreover, to verify the proposed hybrid learning strategy over the different types of cancer disease, another publicly available colon cancer database of histopathology images is collected from Kaggle [36]. The colon database consists of two classes, adenocarcinoma and normal, with a total of 5000 patches per type of size $768 \times 768 \times 3$. Samples of all three datasets are shown in Fig. 3

B. Proposed model architecture

Using transfer learning, we can apply models that have been trained on large diverse datasets (i.e., “pre-trained models”) to smaller, related datasets in a more efficient manner [12], [25], [29], [30], [32], [33]. In general, the pre-trained models have two parts: a feature extractor and a classifier. In transfer learning, the classifier is modified while the feature extractor is left untouched. This is because the pre-trained models are usually trained on the Imagenet dataset with 1000 output classes, while in general, the number of output classes is limited. Therefore, only the last classification layer of the pre-trained model is re-trained and named as “base model”.

In general, the top layers of any pre-trained model’s feature extractor capture the fine details that pertain solely to output classes, and therefore, such top layers are re-trained when fine-tuning the model on small custom datasets to optimize the performance of the model [25], [32], [33]. In contrast to the top layers, the bottom layers capture the more generic features such as lines, edges, and shapes that contribute more to the classification task. Besides the feature extractor and the classifier, another important attribute of the pre-trained model is the depth of the model. There has been evidence that deeper models can improve classification performance, although this is not always the case [17]–[19]. Considering all these aspects, we propose an architecture in which (i) the feature extractor remains unchanged except for a few top layers and (ii) a few more fully connected layers are added before the final classification layer. This modified model is referred to as the “hybrid model”, which combines both the concepts of transfer learning and fine-tuning. The number of additional fully connected layers is decided empirically. The performance of eight different types of pre-trained models such as ResNet50 [17], VGG16 [16], EfficientNetb0 [19], EfficientNetb1 [19], EfficientNetb2 [19], EfficientNetb3 [19], EfficientNetb4 [19], DenseNet121 [18] is compared while designing the hybrid model. Fig. 4 shows the architecture of base and hybrid models.

C. Training

The overall architecture of the proposed model is comprised of two stages: (i) offline system and (ii) online system as shown in Fig. 5. PyTorch framework was used for designing the model. Initially, the pre-processed image patches are divided into training (90%) and testing datasets (10%) as shown in Table I. The image patches are resized to $224 \times 224 \times 3$ pixel dimensions to maintain uniformity across datasets and allow faster and more precise training. The offline system uses the training dataset and performs the 5-fold stratified cross-validation to train the proposed model. In 5-fold cross-validation, the training data is divided into five equal non-overlapping parts. The model is trained on the four parts and validated on the remaining part of the training dataset. Dynamic augmentation is performed on these four training parts of the data with random rotation on the TCGA-LIHC dataset, random rotation with random horizontal flip on the COLON dataset, and random rotation with random horizontal and vertical flip on the KMC dataset. Furthermore, to minimize

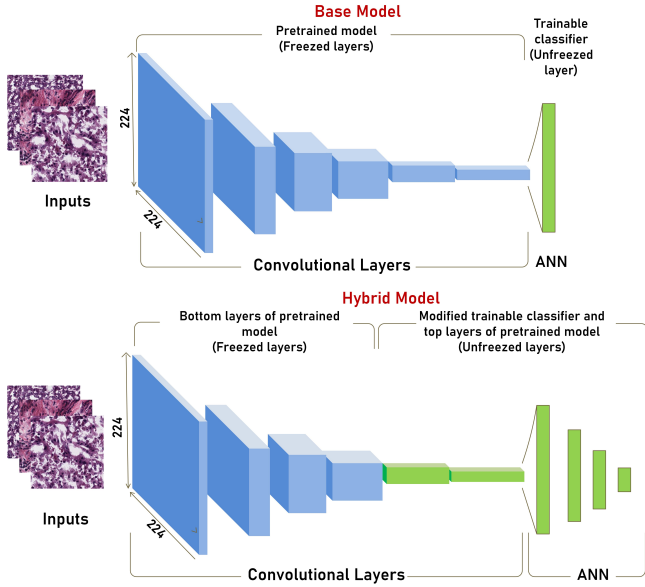


Figure 4. i) base model: All of the convolutional layers in pre-trained model are frozen and the last fully connected layer is replaced and kept trainable. ii) hybrid model: Bottom layers of the convolutional of the pre-trained model are frozen. A shallow classifier is replaced with a deep classifier. classifier and selective top layers of the pre-trained model are kept trainable.

the class imbalance, a weighted random sampler approach [37] is followed that samples images of different classes with pre-defined weights. The weights are inversely utilized based on the number of classes in the training dataset. Both the dynamic augmentation and weighted random sampler methods aid in reducing the class-imbalance effect in the dataset. This complete process is repeated five times in 5-fold cross-validation and an averaged validation performance is recorded. The hyperparameters used while training the model are shown in Table II. Moreover, The cosine annealing warm restart [38] learning rate scheduler is used to select the learning rate over all the epochs. This is mathematically represented in Eq.[1], where, η_{min}^i and η_{max}^i are learning rate ranges. T_{cur} indicates the number of epochs from the last restart, and T_i indicates the number of epochs after which a restart is scheduled. The model is trained for 47 epochs with early stopping criteria and a warm restart of the learning rate scheduler at every 12^{th} epoch (T_i). In this study, an initial learning rate of 0.001 (η_{max}^i) is used.

$$\eta_t = \eta_{min}^i + \frac{1}{2} (\eta_{max}^i - \eta_{min}^i) \left(1 + \cos \left(\frac{T_{cur}}{T_i} \pi \right) \right) \quad (1)$$

Furthermore, the cross entropy loss (L_{CE}) between labels and ground truth values is used, which is defined in Eq.[2]

$$L_{CE} = - \sum_{i=0}^{N-1} y_i \log(p_i) \quad (2)$$

where N is the number of classes, and y_i and p_i are the ground truth values and the predicted probabilistic values, respectively. This loss function is widely preferred over the others. The reason for this is that, if we see the curve of loss

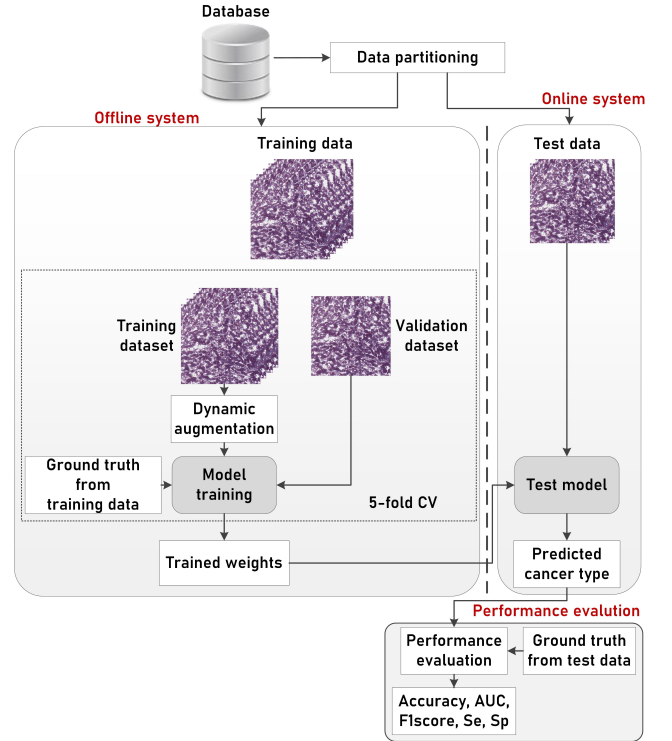


Figure 5. The architecture of the proposed model.

vs. probability, loss is very high when prediction is inaccurate. As a result, the gradient of loss is high, which aids in faster convergence. Once the model is trained, the training weights are used to transform the test dataset into the output cancer types using the test model. The performance of the model is evaluated on the test data using five performance measures such as accuracy, sensitivity, specificity, F1-score, and area under the curve (AUC). The pre-trained models were imported from the Pytorch library and trained on Google Colab.

Table I
NUMBER OF PATCHES AND THEIR DISTRIBUTION

Dataset		Type0	Type1	Type2	Type3	Total
TCGA-LIHC	Train	1098	1206	1224	NA	3528
	Test	122	134	136	NA	392
	Total	1220	1340	1360	NA	3920
KMC	Train	649	719	696	661	2725
	Test	70	80	80	50	280
	Total	719	799	776	711	3005
COLON	Train	4500	4500	NA	NA	9000
	Test	500	500	NA	NA	1000
	Total	5000	5000	NA	NA	10000

D. Performance Metrics

The quantitative performance of the proposed hybrid model was evaluated using a standard protocol such as accuracy, sensitivity, specificity, and F1-score [6], [39]. These performance evaluation metrics were computed using a contingency table that holds positive (TP), false positive (FP), true negative (TN), and false negative (FN). Finally, receiver operating characteristics (ROC) and area under the curve (AUC) [40] were determined. li2019staged

Table II
HYPERPARAMETERS USED DURING TRAINING OF MODELS

Parameter	Value
Batch size	64 or 32
Learning rate	0.001
Optimizer	Adam
Beta1	0.9
Beta2	0.999
Epochs	47
Learning rate scheduler	Cosine annealing warm restart
Warm Restart	12
Loss	Cross entropy loss

III. RESULTS

In this study, the proposed hybrid model is independently trained and evaluated on the TCGA-LIHC, KMC and COLON datasets as per the strategy discussed in the ‘‘Training’’ section. The training and validation accuracy along with the training and validation loss are plotted for all the datasets. The five performance metrics namely accuracy, sensitivity, specificity, F1-score and AUC for each model were averaged over five-folds and presented in this section along with the ROC curves and confusion matrix attributed to respective folds.

A. Results on TCGA-LIHC dataset

To investigate the training and validation performance of the proposed hybrid model, the training, validation accuracy and loss are shown in Fig. 6 and Fig. 7, respectively. It has been observed that the difference between training and validation accuracy reduces with the progression of epochs indicating proper training in the absence of both bias and variance. Furthermore, the consistent decrease in the training and validation loss indicates that the model is learning at every epoch and once the model is trained, both the curves remain unchanged. Fig. 8 and Fig. 9 show the confusion matrices and the ROC curves for all the five folds. Both these figures show accurate prediction of patches with and without liver cancer. Table III and Table IV show the performance metrics using the base model and the proposed hybrid model, respectively. It has been observed that all the models with the proposed hybrid strategy have resulted in better prediction of cancer grading compared to the base model. The hybrid ResNet50 model provided an increment of 1.74% (100% vs. 98.26%) over the base ResNet50 model. Similarly, the other performance metrics such as sensitivity, specificity, and F1-score also provided the prediction performance of 100% with an AUC of unity. The results indicate that the hybrid learning strategy can avoid false predictions justifying the robustness of the model.

B. Results on KMC dataset

The training and validation accuracy and loss are shown in Fig. 10 and Fig. 11, respectively. Here as well proper training in the absence of both bias and variance can be observed. Furthermore, the consistent decrease in the training and validation loss indicates that the model is learning at every epoch and once the model is trained, both the curves saturate. Fig. 12 and Fig. 13 show the confusion matrices and the

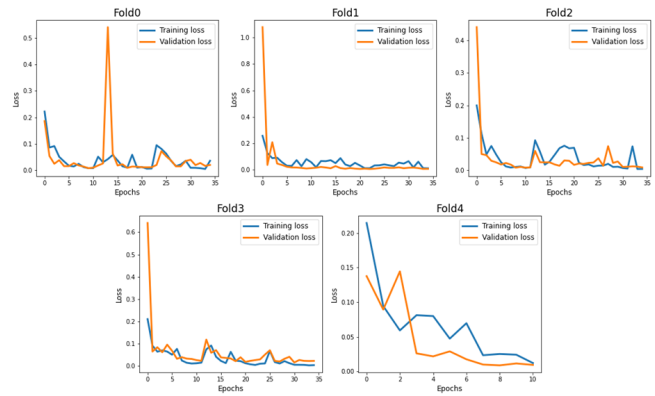


Figure 6. Train and validation loss plotted for all epochs, all 5 folds over TCGA train dataset of hybrid model with ResNet50 as feature extractor

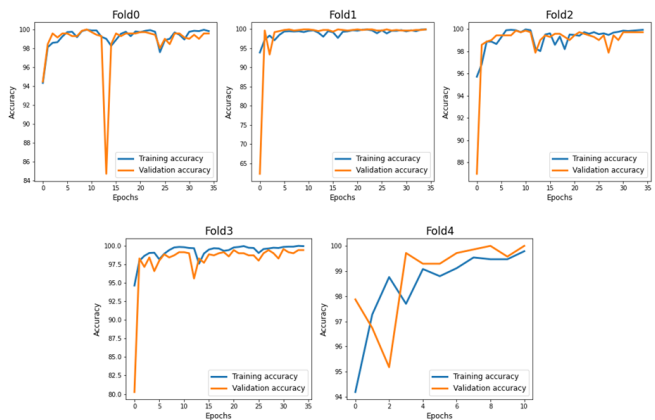


Figure 7. Train and validation accuracy plotted for all epochs, all 5 folds over TCGA train dataset of hybrid model with ResNet50 as feature extractor

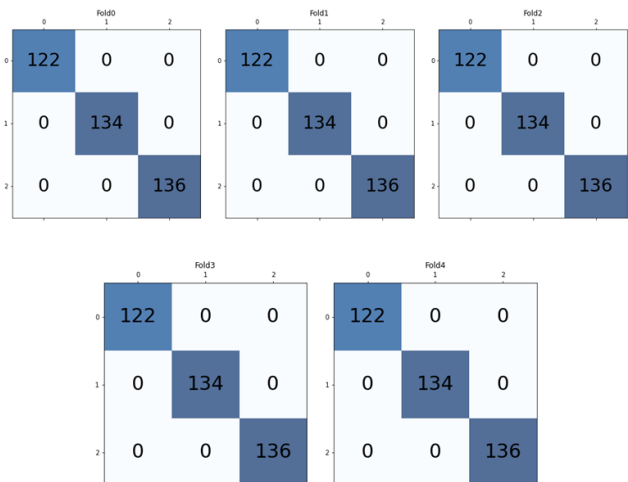


Figure 8. Confusion matrix of all 5 folds over TCGA test dataset of trained hybrid model with ResNet50 as feature extractor

ROC curves for all five folds. Table V and Table VI show the performance metrics using the base model and the proposed hybrid model, respectively over the KMC dataset. The results for KMC dataset also show that the proposed hybrid strategy has resulted in better prediction of cancer grading compared

Table III
THE PERFORMANCE METRICS OF BASE MODELS CALCULATED ON TCGA-LIHC TEST DATASET.

Metrics		ResNet50	VGG16	EfficientNetb0	EfficientNetb1	EfficientNetb2	EfficientNetb3	EfficientNetb4	DenseNet121
Accuracy		98.26±0.11	98.51±0.48	98.92±0.49	97.19±0.59	98.41±0.37	94.48±0.49	95.35±0.75	97.49±0.21
F1-score	Type0	99.59±0.00	99.91±0.18	99.59±0.00	99.59±0.40	100.00±0.00	99.09±0.18	99.42±0.37	100.00±0.00
	Type1	97.51±0.16	97.86±0.69	98.44±0.69	95.84±0.89	97.66±0.57	92.33±0.88	93.69±0.94	96.43±0.29
	Type2	97.82±0.17	97.91±0.62	98.81±0.71	96.36±0.74	97.74±0.53	92.50±0.57	93.36±0.98	96.30±0.32
	Weighted avg	98.27±0.11	98.51±0.48	98.93±0.48	97.19±0.59	98.41±0.37	94.49±0.49	95.36±0.74	97.49±0.21
Specificity	Type0	100.00±0.00	100.00±0.00	100.00±0.00	99.77±0.20	100.00±0.00	99.70±0.16	100.00±0.00	100.00±0.00
	Type1	97.51±0.20	98.14±0.63	98.75±0.74	98.45±0.47	99.22±0.00	95.34±0.61	94.49±1.35	96.74±0.34
	Type2	99.84±0.21	99.61±0.27	99.61±0.00	97.50±0.76	98.36±0.57	96.56±0.64	98.44±0.55	99.45±0.21
	Macro avg	99.12±0.05	99.25±0.24	99.45±0.24	98.57±0.30	99.19±0.19	97.20±0.25	97.64±0.38	98.73±0.10
Sensitivity	Type0	99.18±0.00	99.83±0.36	99.18±0.00	99.67±0.44	100.00±0.00	98.85±0.44	98.85±0.73	100.00±0.00
	Type1	99.70±0.41	99.25±0.52	99.25±0.00	94.77±1.39	96.86±1.10	93.43±1.22	97.46±0.85	98.95±0.40
	Type2	96.02±0.39	96.61±0.98	98.38±1.41	97.35±0.65	98.53±0.00	91.62±0.65	90.14±2.11	93.82±0.65
	Macro avg	98.30±0.11	98.56±0.48	98.93±0.47	97.26±0.58	98.46±0.36	94.63±0.49	95.48±0.74	97.59±0.20
AUC	Type0	1.00±0.00	1.00±0.00	1.00±0.00	0.99±0.00	1.00±0.00	0.99±0.00	1.00±0.00	1.00±0.00
	Type1	0.99±0.00	0.99±0.00	0.99±0.00	0.99±0.00	0.99±0.00	0.98±0.00	0.99±0.00	0.99±0.00
	Type2	0.99±0.00	0.99±0.00	0.99±0.00	0.99±0.00	0.99±0.00	0.99±0.00	0.99±0.00	0.99±0.00
	Macro avg	0.99±0.00	0.99±0.00	0.99±0.00	0.99±0.00	0.99±0.00	0.99±0.00	0.99±0.00	0.99±0.00

*All metrics except AUC are expressed in percentages.

Table IV
THE PERFORMANCE METRICS OF HYBRID MODELS CALCULATED ON TCGA-LIHC TEST DATASET.

Metrics		ResNet50	VGG16	EfficientNetb0	EfficientNetb1	EfficientNetb2	EfficientNetb3	EfficientNetb4	DenseNet121
Accuracy		100.00±0.00	99.43±0.49	99.89±0.14	99.94±0.11	99.89±0.22	99.74±0.18	99.74±0.18	99.59±0.53
f1-score	class 0	100.00±0.00	99.83±0.37	100.00±0.00	100.00±0.00	100.00±0.00	99.91±0.18	100.00±0.00	100.00±0.00
	class 1	100.00±0.00	99.18±0.71	99.85±0.20	99.92±0.16	99.85±0.33	99.63±0.26	99.62±0.26	99.40±0.77
	class 2	100.00±0.00	99.33±0.48	99.85±0.20	99.92±0.16	99.85±0.33	99.70±0.30	99.63±0.26	99.40±0.77
	macro avg	100.00±0.00	99.45±0.48	99.90±0.13	99.95±0.11	99.90±0.21	99.75±0.17	99.75±0.17	99.60±0.51
	weighted avg	100.00±0.00	99.43±0.48	99.89±0.14	99.94±0.11	99.89±0.22	99.74±0.18	99.74±0.18	99.59±0.53
Specificity	class 0	100.00±0.00	100.00±0.00	100.00±0.00	100.00±0.00	100.00±0.00	99.92±0.16	100.00±0.00	100.00±0.00
	class 1	100.00±0.00	99.45±0.64	99.92±0.17	100.00±0.00	99.92±0.17	99.68±0.32	99.84±0.21	99.53±0.69
	class 2	100.00±0.00	99.68±0.17	99.92±0.17	99.92±0.17	99.92±0.17	100.00±0.00	99.76±0.21	99.84±0.21
	macro avg	100.00±0.00	99.71±0.24	99.94±0.07	99.97±0.05	99.94±0.11	99.87±0.09	99.87±0.09	99.79±0.27
	weighted avg	100.00±0.00	99.71±0.24	99.94±0.07	99.97±0.05	99.94±0.11	99.87±0.09	99.87±0.09	99.79±0.27
Sensitivity	class 0	100.00±0.00	99.67±0.73	100.00±0.00	100.00±0.00	100.00±0.00	100.00±0.00	100.00±0.00	100.00±0.00
	class 1	100.00±0.00	99.40±0.33	99.85±0.33	99.85±0.33	99.85±0.33	99.85±0.33	99.55±0.41	99.70±0.41
	class 2	100.00±0.00	99.26±0.73	99.85±0.33	100.00±0.00	99.85±0.33	99.41±0.61	99.70±0.40	99.11±1.31
	macro avg	100.00±0.00	99.44±0.49	99.90±0.13	99.95±0.11	99.90±0.22	99.75±0.17	99.75±0.17	99.60±0.51
	weighted avg	100.00±0.00	99.44±0.49	99.90±0.13	99.95±0.11	99.90±0.22	99.75±0.17	99.75±0.17	99.60±0.51
AUC	class 0	1.00±0.00	1.00±0.00	1.00±0.00	1.00±0.00	1.00±0.00	1.00±0.00	1.00±0.00	1.00±0.00
	class 1	1.00±0.00	0.99±0.00	1.00±0.00	1.00±0.00	1.00±0.00	1.00±0.00	0.99±0.00	0.99±0.00
	class 2	1.00±0.00	0.99±0.00	1.00±0.00	1.00±0.00	1.00±0.00	1.00±0.00	0.99±0.00	0.99±0.00
	macro avg	1.00±0.00	0.99±0.00	1.00±0.00	1.00±0.00	1.00±0.00	1.00±0.00	0.99±0.00	0.99±0.00
	weighted avg	1.00±0.00	0.99±0.00	1.00±0.00	1.00±0.00	1.00±0.00	1.00±0.00	0.99±0.00	0.99±0.00

*All metrics except AUC are expressed in percentages.

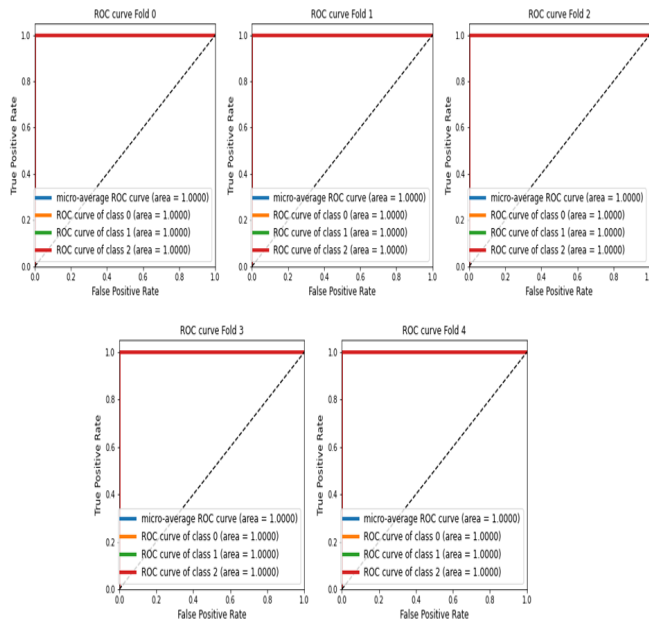


Figure 9. ROC curve of all 5 folds over TCGA test dataset of trained hybrid model with ResNet50 as a feature extractor.

to the base model. The hybrid EfficientNet3 achieves 96.71% accuracy with a 2.22% standard deviation. This is an increment of 4.65% over the base EfficientNet3 model.

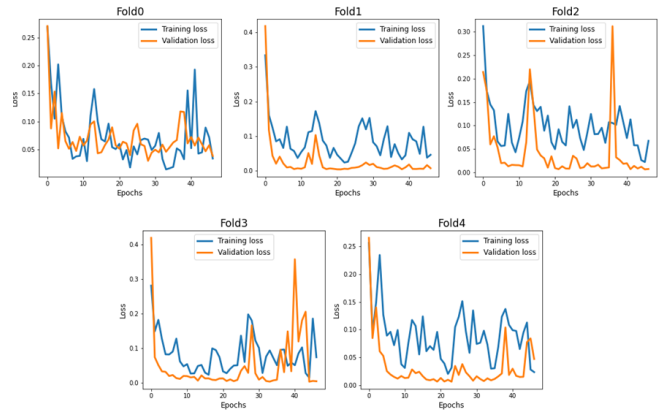


Figure 10. Train and validation loss plotted for all epochs, all 5 folds over KMC train dataset of hybrid model with EfficientNetb3 as feature extractor

Table V
THE PERFORMANCE METRICS OF BASE MODELS CALCULATED ON KMC TEST DATASET.

Metrics		ResNet50	VGG16	EfficientNetb0	EfficientNetb1	EfficientNetb2	EfficientNetb3	EfficientNetb4	DenseNet121
Accuracy		88.28±0.63	87.35±0.59	91.49±0.73	92.57±0.77	88.28±1.32	92.07±0.81	90.42±0.68	89.78±0.85
F1-score	Type0	100.00±0.00	100.00±0.00	99.29±0.00	99.85±0.31	99.14±0.32	99.00±0.38	98.85±1.08	100.00±0.00
	Type1	81.70±0.83	83.75±1.49	86.78±1.18	88.51±0.88	81.18±2.06	88.23±0.64	87.07±1.13	84.52±1.62
	Type2	84.87±1.36	78.65±1.12	86.55±1.05	87.18±1.44	79.78±1.82	86.91±1.25	86.09±1.04	87.19±1.16
	Type3	88.89±0.00	89.37±0.66	96.26±0.96	97.53±0.95	98.16±0.86	96.89±1.31	91.30±0.00	88.64±0.55
	Weighted avg	88.46±0.62	87.36±0.59	91.53±0.72	92.57±0.77	88.30±1.27	92.09±0.81	90.49±0.68	89.89±0.82
Specificity	Type0	100.00±0.00	100.00±0.00	99.52±0.00	99.90±0.21	99.52±0.00	99.42±0.21	99.61±0.39	100.00±0.00
	Type1	87.00±0.86	87.50±2.29	93.70±0.27	91.50±0.50	91.30±0.57	94.90±0.82	94.10±0.41	88.90±1.14
	Type2	96.60±0.22	94.80±2.01	94.90±1.08	98.20±0.75	92.80±2.07	94.60±0.54	92.90±0.82	96.80±0.44
	Type3	100.00±0.00	100.00±0.00	100.00±0.00	100.00±0.00	100.00±0.00	100.00±0.00	100.00±0.00	100.00±0.00
	Macro avg	95.90±0.22	95.57±0.20	97.03±0.25	97.40±0.27	95.90±0.46	97.23±0.28	96.65±0.23	96.42±0.30
Sensitivity	Type0	100.00±0.00	100.00±0.00	100.00±0.00	100.00±0.00	99.71±0.63	99.71±0.63	98.85±1.19	100.00±0.00
	Type1	91.50±0.55	94.50±2.59	88.75±2.33	96.25±0.88	83.25±4.10	89.00±1.04	88.50±2.40	93.50±1.62
	Type2	80.00±2.16	73.25±3.37	86.00±1.04	80.75±1.11	78.25±1.42	87.25±2.05	89.00±1.04	83.50±1.85
	Type3	80.00±0.00	80.80±1.09	92.80±1.78	95.20±1.78	96.40±1.67	94.00±2.44	84.00±0.00	79.60±0.89
	Macro avg	87.87±0.55	87.13±0.52	91.88±0.79	93.05±0.82	89.40±1.30	92.49±0.92	90.08±0.61	89.15±0.82
AUC	Type0	1.00±0.00	1.00±0.00	1.00±0.00	1.00±0.00	0.99±0.00	1.00±0.00	0.99±0.00	1.00±0.00
	Type1	0.96±0.00	0.96±0.00	0.98±0.00	0.98±0.00	0.96±0.00	0.98±0.00	0.98±0.00	0.97±0.00
	Type2	0.97±0.00	0.95±0.00	0.98±0.00	0.97±0.00	0.95±0.00	0.97±0.00	0.97±0.00	0.98±0.00
	Type3	0.98±0.00	0.99±0.00	0.99±0.00	1.00±0.00	0.99±0.00	0.99±0.00	0.99±0.00	0.99±0.00
	Macro avg	0.98±0.00	0.98±0.00	0.99±0.00	0.99±0.00	0.98±0.00	0.99±0.00	0.99±0.00	0.98±0.00

*All metrics except AUC are expressed in percentages.

Table VI
THE PERFORMANCE METRICS OF HYBRID MODELS CALCULATED ON KMC TEST DATASET.

Metrics		ResNet50	VGG16	EfficientNetb0	EfficientNetb1	EfficientNetb2	EfficientNetb3	EfficientNetb4	DenseNet121
Accuracy		95.07±2.13	90.64±1.24	96.21±1.81	96.14±2.24	95.49±2.22	96.71±0.68	96.49±2.41	94.92±1.14
F1-score	Type0	98.79±2.70	99.29±0.70	99.58±0.93	100.00±0.00	100.00±0.00	100.00±0.00	100.00±0.00	99.58±0.94
	Type1	93.01±1.69	88.74±2.41	94.48±1.83	94.76±3.12	93.40±2.75	94.91±1.41	97.70±1.66	94.26±2.12
	Type2	93.35±2.43	85.95±3.84	92.90±3.51	94.02±2.99	93.65±3.98	94.33±0.76	94.25±3.93	92.40±3.02
	Type3	95.80±5.76	88.75±1.83	99.38±1.38	96.38±3.51	95.42±5.09	98.78±1.32	92.96±5.06	93.24±4.39
	Weighted avg	95.05±2.17	90.58±1.24	96.17±1.85	96.15±2.22	95.48±2.23	96.71±0.66	96.44±2.46	94.88±1.16
Specificity	Type0	99.14±1.91	99.52±0.47	99.71±0.63	100.00±0.00	100.00±0.00	100.00±0.00	100.00±0.00	99.71±0.64
	Type1	95.00±2.00	91.60±1.29	95.30±1.64	95.50±2.85	94.40±2.67	95.70±1.25	98.10±1.38	95.10±1.92
	Type2	99.00±1.17	96.50±1.36	99.70±0.67	99.10±1.24	99.30±0.57	99.90±0.22	97.00±2.15	98.10±2.07
	Type3	100.00±0.00	99.39±0.72	100.00±0.00	100.00±0.00	100.00±0.00	99.82±0.38	100.00±0.00	100.00±0.00
	Macro avg	98.28±0.72	96.75±0.43	98.67±0.62	98.65±0.78	98.42±0.77	98.85±0.24	98.77±0.84	98.22±0.40
Sensitivity	Type0	100.00±0.00	100.00±0.00	100.00±0.00	100.00±0.00	100.00±0.00	100.00±0.00	100.00±0.00	100.00±0.00
	Type1	97.75±2.56	96.50±2.40	100.00±0.00	100.00±0.00	99.75±0.55	100.00±0.00	100.00±0.00	100.00±0.00
	Type2	89.75±3.89	82.00±4.47	87.50±5.07	90.75±3.81	89.75±5.95	89.50±1.11	95.75±2.87	90.00±5.45
	Type3	92.40±10.43	82.00±2.00	98.80±2.68	93.20±6.57	91.60±9.20	98.40±2.60	87.20±9.01	87.60±7.92
	Macro avg	94.97±2.73	90.12±0.91	96.57±1.79	95.98±2.58	95.27±2.61	96.97±0.83	95.73±2.95	94.40±1.40
AUC	Type0	1.00±0.00	1.00±0.00	1.00±0.00	1.00±0.00	1.00±0.00	1.00±0.00	1.00±0.00	1.00±0.00
	Type1	0.98±0.01	0.98±0.00	0.99±0.00	0.99±0.00	0.99±0.00	0.99±0.00	0.99±0.00	0.99±0.00
	Type2	0.98±0.02	0.97±0.00	0.99±0.00	0.99±0.00	0.99±0.00	0.99±0.00	0.99±0.00	0.99±0.00
	Type3	0.99±0.00	0.98±0.01	1.00±0.00	1.00±0.00	0.99±0.00	0.99±0.00	0.99±0.00	0.99±0.00
	Macro avg	0.99±0.00	0.98±0.00	0.99±0.00	0.99±0.00	0.99±0.00	0.99±0.00	0.99±0.00	0.99±0.00

*All metrics except AUC are expressed in percentages.

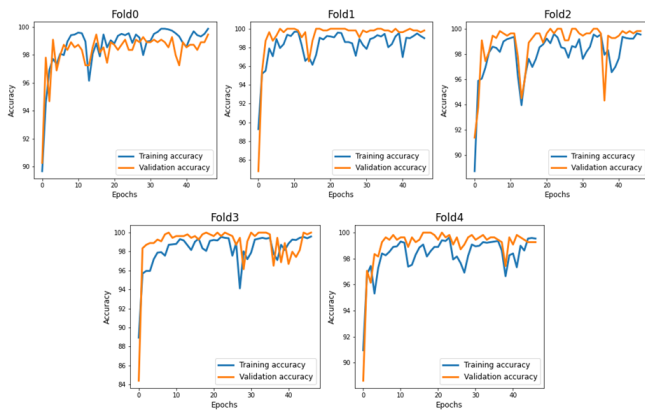


Figure 11. Train and validation accuracy plotted for all epochs, all 5 folds over KMC train dataset of hybrid model with EfficientNetb3 as feature extractor

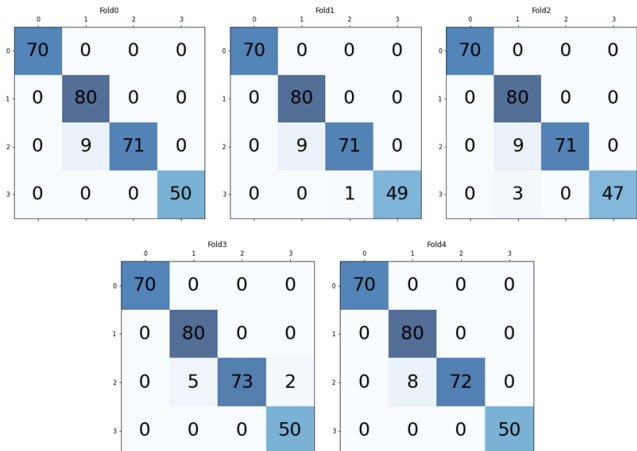


Figure 12. Confusion matrix of all 5 folds over KMC test dataset of trained hybrid model with EfficientNetb3 as feature extractor

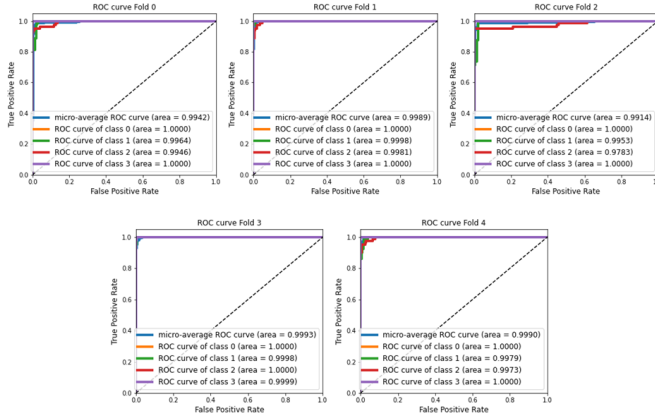


Figure 13. ROC curve of all 5 folds over KMC test dataset of trained hybrid model with EfficientNetb3 as feature extractor.

C. Results on COLON dataset

To assess the performance of the proposed hybrid model, colon dataset is also considered. Fig. 14 and Fig. 15 show the confusion matrices and the ROC curves for all five folds. Table VII and Table VIII show the performance metrics using the base model and the proposed hybrid model, respectively over the COLON dataset. Hybrid models are found to perform better for this database as well. The hybrid EfficientNet2, EfficientNet4 and DenseNet121 achieve 100% accuracy. This is an increment of 0.44, 0.36, and 0.32% over the base models respectively.

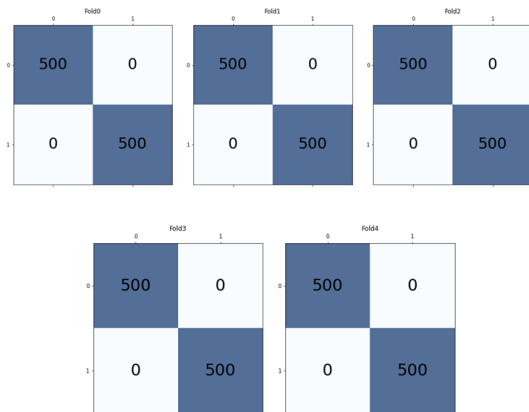


Figure 14. Confusion matrix of all 5 folds over COLON test dataset of trained hybrid model with DenseNet121 as feature extractor

IV. DISCUSSION

The goal of this study is to develop a methodology for classifying different types of liver HCC tumors. We designed a deep learning-based hybrid architecture, trained and tested over two liver HCC datasets. The different data pre-processing steps along with training and validation techniques are also incorporated to build a robust model. After training the models, performance metrics over the test dataset were generated and observed. In this section, conclusions made from the obtained results, a comparison of the proposed methodology with

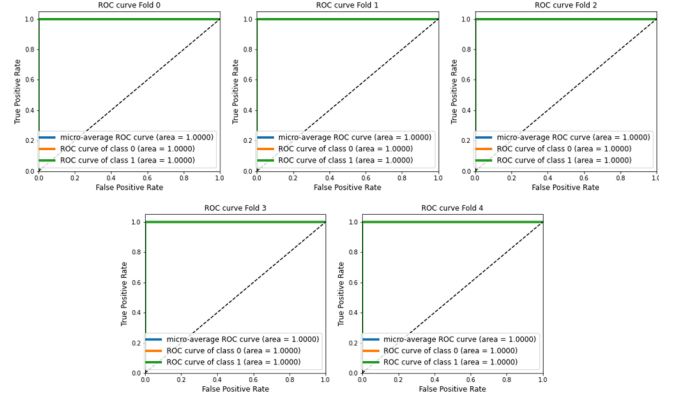


Figure 15. ROC curve of all 5 folds over COLON test dataset of trained hybrid model with DenseNet121 as feature extractor

recent studies and limitations of the proposed methodology are mentioned.

We observe that hybrid models perform better than base models for all datasets mentioned above. Hybrid models show a minimum 0.76% (VGG16) and 3.29% (VGG16) of hike in accuracy on TCGA and KMC datasets respectively. The hybrid model with ResNet50 as a feature extractor outperforms the others on TCGA, achieving 100% accuracy with a 1.74% increase after modification (Tables III, IV) for TCGA dataset. Performance metrics indicate the excellent ability of classification and the robustness of the model. The hybrid model with EfficientNet3 outperforms all other models on KMC in terms of every performance metric (Tables V, VI). With an accuracy of 96.71% and a 2.22% standard deviation, this model sets the benchmark for KMC database. A similar trend is observed for the COLON dataset as well. The hybrid models with EfficientNet2, EfficientNet4 and DenseNet121 feature extractors show remarkable performance by achieving 100% accuracy on the test dataset. These results prove that replacing a shallow classifier with a deep classifier and fine-tuning the top layers of the feature extractor is a fruitful strategy.

For the TCGA dataset, the base model with EfficientNet0 as a feature extractor gives better accuracy, whereas, among the hybrid models, ResNet50 is proven to be the best. On the other hand, for the KMC dataset, EfficientNet3 outperforms other architectures. Various architectures are observed to produce the best performance across the datasets. This concludes the data specificity of deep architectures and not model specificity. Various architectures are designed in a way to identify or detect certain types of features that are associated with particular datasets, even when the tissues are those of the liver, but share different genetic patterns and different ways of WSI preparation procedures.

Some recent studies on liver HCC detection involving the TCGA and KMC datasets are mentioned in Table IV. As can be seen, the proposed methodology outperforms other studies on local image classification tasks in terms of accuracy as well as other performance metrics. LiverNet architecture [2] claimed the best performance over KMC and TCGA datasets in the patch-level classification task. The LiverNet model

Table VII
THE PERFORMANCE METRICS OF BASE MODELS CALCULATED ON COLON TEST DATASET.

Metrics		ResNet50	VGG16	EfficientNetb0	EfficientNetb1	EfficientNetb2	EfficientNetb3	EfficientNetb4	DenseNet121
Accuracy		99.54±0.13	99.94±0.05	99.90±0.07	99.70±0.07	99.56±0.18	99.84±0.05	99.74±0.09	99.68±0.18
F1-score	Type0	99.54±0.13	99.94±0.05	99.90±0.07	99.70±0.07	99.56±0.18	99.84±0.05	99.74±0.09	99.68±0.18
	Type1	99.54±0.13	99.94±0.05	99.90±0.07	99.70±0.07	99.56±0.18	99.84±0.05	99.74±0.09	99.68±0.18
	Weighted avg	99.54±0.13	99.94±0.05	99.90±0.07	99.70±0.07	99.56±0.18	99.84±0.05	99.74±0.09	99.68±0.18
Specificity	Type0	100.00±0.00	100.00±0.00	100.00±0.00	99.80±0.00	99.80±0.00	100.00±0.00	100.00±0.00	100.00±0.00
	Type1	99.08±0.27	99.88±0.11	99.80±0.14	99.60±0.14	99.32±0.36	99.68±0.11	99.48±0.18	99.36±0.36
	Macro avg	99.54±0.13	99.94±0.05	99.90±0.07	99.70±0.07	99.56±0.18	99.84±0.05	99.74±0.09	99.68±0.18
Sensitivity	Type0	99.08±0.27	99.88±0.11	99.80±0.14	99.60±0.14	99.32±0.36	99.68±0.11	99.48±0.18	99.36±0.36
	Type1	100.00±0.00	100.00±0.00	100.00±0.00	99.80±0.00	99.80±0.00	100.00±0.00	100.00±0.00	100.00±0.00
	Macro avg	99.54±0.13	99.94±0.05	99.90±0.07	99.70±0.07	99.56±0.18	99.84±0.05	99.74±0.09	99.68±0.18
AUC	Type0	1.00±0.00	1.00±0.00	1.00±0.00	1.00±0.00	1.00±0.00	1.00±0.00	1.00±0.00	1.00±0.00
	Type1	1.00±0.00	1.00±0.00	1.00±0.00	1.00±0.00	1.00±0.00	1.00±0.00	1.00±0.00	1.00±0.00
	Macro avg	1.00±0.00	1.00±0.00	1.00±0.00	1.00±0.00	1.00±0.00	1.00±0.00	1.00±0.00	1.00±0.00

*All metrics except AUC are expressed in percentages.

Table VIII
THE PERFORMANCE METRICS OF HYBRID MODELS CALCULATED ON COLON TEST DATASET.

Metrics		ResNet50	VGG16	EfficientNetb0	EfficientNetb1	EfficientNetb2	EfficientNetb3	EfficientNetb4	DenseNet121
Accuracy		99.96±0.05	99.96±0.05	99.98±0.04	99.98±0.04	100.00±0.00	99.90±0.17	100.00±0.00	100.00±0.00
F1-score	Type0	99.96±0.05	99.96±0.05	99.98±0.04	99.98±0.04	100.00±0.00	99.90±0.17	100.00±0.00	100.00±0.00
	Type1	99.96±0.05	99.96±0.05	99.98±0.04	99.98±0.04	100.00±0.00	99.90±0.17	100.00±0.00	100.00±0.00
	Weighted avg	99.96±0.05	99.96±0.05	99.98±0.04	99.98±0.04	100.00±0.00	99.90±0.17	100.00±0.00	100.00±0.00
Specificity	Type0	100.00±0.00	100.00±0.00	100.00±0.00	100.00±0.00	100.00±0.00	100.00±0.00	100.00±0.00	100.00±0.00
	Type1	99.92±0.11	99.92±0.11	99.96±0.08	99.96±0.09	100.00±0.00	99.80±0.35	100.00±0.00	100.00±0.00
	Macro avg	99.96±0.05	99.96±0.05	99.98±0.04	99.98±0.04	100.00±0.00	99.90±0.17	100.00±0.00	100.00±0.00
Sensitivity	Type0	99.92±0.11	99.92±0.11	99.96±0.08	99.96±0.09	100.00±0.00	99.80±0.35	100.00±0.00	100.00±0.00
	Type1	100.00±0.00	100.00±0.00	100.00±0.00	100.00±0.00	100.00±0.00	100.00±0.00	100.00±0.00	100.00±0.00
	Macro avg	99.96±0.05	99.96±0.05	99.98±0.04	99.98±0.04	100.00±0.00	99.90±0.17	100.00±0.00	100.00±0.00
AUC	Type0	1.00±0.00	1.00±0.00	1.00±0.00	1.00±0.00	1.00±0.00	1.00±0.00	1.00±0.00	1.00±0.00
	Type1	1.00±0.00	1.00±0.00	1.00±0.00	1.00±0.00	1.00±0.00	1.00±0.00	1.00±0.00	1.00±0.00
	Macro avg	1.00±0.00	1.00±0.00	1.00±0.00	1.00±0.00	1.00±0.00	1.00±0.00	1.00±0.00	1.00±0.00

*All metrics except AUC are expressed in percentages.

has some key features such as CBAM, ASPP block and hypercolumn technique, which take care of a lesser number of model parameters and show improved performance. Our proposed methodology exceeds LiverNet’s accuracy by more than 2% over the TCGA dataset and by more than 5% on the KMC dataset, despite having less number of patches in the KMC dataset. LiverNet achieves F1-score of 97.72% and 90.93%. On the other hand, our methodology achieves 100% and 96.446% F1-score on TCGA and KMC respectively. They had also produced results using a very similar architecture called BreastNet [20] which was specifically designed for breast cancer classification over breakhis dataset [41]. Our proposed model outperforms BreastNet as well.

Chen et al. [13] used pre-trained InceptionV3 which achieves low accuracy (89.6%) despite having a large number of parameters. They trained the model using a massive dataset containing approximately 39k train patches. Sun et al. [12] used pre-trained ResNet50 for patch-level feature extraction. They proposed a global-level (whole slide image level) classification mechanism based on the selection of k -top and k -bottom features from a sorted aggregation of patch-level features. On the other hand, our research focuses on patch-level classification. For aggregation, Sun et al. performed p-norm pooling, and for the classification of $2k$ features, they trained a multi-layered perceptron. The k value was chosen experimentally. For only two-class classification at the global level, this study claimed 100% accuracy.

For 3-class patch-level classification on TCGA and 2-class patch-level classification on KMC datasets, the proposed hybrid methodology outperforms all the above-mentioned stud-

ies. Furthermore, the proposed model achieves better performance despite being trained on a comparatively smaller dataset and provides end-to-end deep learning-based solutions. The performance metrics also indicate the robustness of proposed models over others. We have also demonstrated the performance of our methodology over colon histopathology images. Here as well hybrid models have achieved 100% accuracy.

There are some limitations to this study. ResNet50, EfficientNetb3, and DenseNet121-based architectures have around 25M, 12.5M and 7M parameters, respectively. These models have a large number of parameters, which makes them hard to run on low-end processor specifications. We will try to overcome this limitation in future work and provide a highly accurate and lightweight solution.

V. CONCLUSION

This study was focused on liver HCC classification using histopathology images. The primary dataset TCGA-LIHC was prepared through pre-processing steps involving patch extraction, color normalization and augmentation techniques. Another proprietary KMC dataset and a publically available COLON dataset were used for validation purposes. Through this study, we proposed a deep learning-based hybrid architecture for the classification of liver HCC efficiently and robustly. From the experimental results, it is also observed that the proposed hybrid model outperforms the base model and other state-of-the-art models by a significant margin. The best results on the TCGA dataset were obtained by a hybrid model with ResNet50 as the feature extractor, giving an accuracy of 100±0.00 whereas on the KMC dataset, the proposed hybrid

Table IX

COMPARISON WITH RECENT STUDIES ON HCC LIVER CANCER HISTOPATHOLOGY IMAGES (I) INDICATED THE AUTHOR AND YEAR OF PUBLICATION IN THE FIRST COLUMN. (II) DATASET SPECIFICATIONS. (III) THE NUMBER OF CANCER TYPES INTO WHICH IT WAS CLASSIFIED. (IV) MODEL SPECIFICATIONS. (V) PERFORMANCE METRICS USED IN THAT PARTICULAR STUDY. (VI) TRAINING METHOD (VII) REMARKS SHOW SOME SPECIAL CHARACTERISTICS OF THE MODEL ARCHITECTURE AND METHODOLOGY.

First Author(year)	Dataset	Types	Model	Metrics	Training method	Remark
Sun et al. (2019) [12]	TCGA 189,531 train, patches 224x224 tested over 70WSI	2	Pretrained ResNet50	Accuracy 100 Precision 100 Recall 100 F1-score 100	10 fold CV ^b	Transfer learning, k feature selection from sorted aggregated patch features, global level classification
Chen et al. (2020) [13]	TCGA 39k train, patches, 9k test 256 × 256	3	Pretrained Inceptionv3	Accuracy 89.6 Precision 87.9 Recall 77.1 F1-score 82.0 MCC ^a 0.912	0.85:0.15 train test split	Transfer learning, EasyDL framework very big train set Huge number of parameters
Aatresh et al. (2021) [2]	TCGA 2240 train 140 test 224x224	3	LiverNet	Accuracy 97.72 Precision 97.72 Recall 97.72 F1-score 97.72 IOU ^c 95.61	5 fold CV	Architecture specific for HCC liver cancer classification. CBAM, ASPP block hypercolumn technique less number of parameters
Aatresh et al. (2021) [2]	TCGA 2240 train 140 test 224x224	3	BreastNet	Accuracy 96.04 Precision 96.04 Recall 96.04 F1-score 96.04 IOU 92.47	5 fold CV	Architecture specific for Breast cancer classification. CBAM block hypercolumn technique less number of parameters
Aatresh et al. (2021) [2]	KMC 3210 train 272 test 224x224	2	LiverNet	Accuracy 90.93 Precision 90.93 Recall 90.93 F1-score 90.93 IOU 83.6	5 fold CV	Architecture specific for HCC Liver cancer classification. CBAM, ASPP block hypercolumn technique
Aatresh et al. (2021) [2]	KMC 3210 train 272 test 224x224	2	BreastNet	Accuracy 88.41 Precision 88.41 Recall 88.41 F1-score 88.41 IOU 79.73	5 fold CV	Architecture specific for Breast cancer classification. CBAM block hypercolumn technique
Proposed Hybrid ResNet50 (2022)	TCGA 3528 train 392 test 224x224	3	Pretrained Hybrid ResNet50	Accuracy 100.00 Sensitivity 100.00 Specificity 100.00 F1-score 100.00 AUC 1.00	5 fold CV	Transfer learning, fine tuning, deep classifier training of selective top layer of base model
Proposed hybrid EfficientNetb3 (2022)	KMC 2725 train 280 test 224x224	2	Pretrained Hybrid EfficientNetb3	Accuracy 96.71 Sensitivity 96.97 Specificity 98.85 F1-score 96.71 AUC 0.99	5 fold CV	Transfer learning, fine tuning, deep classifier training of selective top layer of base model

^aMCC stands for Matthews's correlation coefficient. ^bCV stands for Cross Validation. ^cIOU stands for intersection over union

model with EfficientNetb3 as a feature extractor achieves an accuracy of $96.71 \pm 0.68\%$. Moreover, the proposed hybrid models provide outstanding results on the COLON dataset as well. The results lead us to the conclusion that deepening the classifier and customizing the top layers of the feature extractor can help improve performance significantly.

Despite having limitations of model parameters, since many labs are now equipped with high-end systems and because perfect predictions trump computational complexity in the medical domain due to the life-and-death situation, we believe a large number of parameters should not be a major issue.

REFERENCES

- [1] B. J. Erickson, S. Kirk, Y. Lee, O. Bathe, M. Kearns, C. Gerdes, K. Rieger-Christ, and J. Lemmerman, "The cancer genome atlas liver hepatocellular carcinoma collection (TCGA-LIHC)," 2016.
- [2] A. A. Aatresh, K. Alabhya, S. Lal, J. Kini, and P. Saxena, "Livernet: efficient and robust deep learning model for automatic diagnosis of subtypes of liver hepatocellular carcinoma cancer from h&e stained liver histopathology images," *Int J Comput Assist Radiol Surg*, vol. 16, no. 9, pp. 1549–1563, 2021.
- [3] H. B. El-Serag and K. L. Rudolph, "Hepatocellular carcinoma: epidemiology and molecular carcinogenesis," *Gastroenterology*, vol. 132, pp. 2557–2576, June 2007.
- [4] "Key statistics about liver cancer."
- [5] H. Rungay, J. Ferlay, C. de Martel, D. Georges, A. S. Ibrahim, R. Zheng, W. Wei, V. E. Lemmens, and I. Soerjomataram, "Global, regional and national burden of primary liver cancer by subtype," *Eur. J. Cancer*, vol. 161, pp. 108–118, 2022.
- [6] X. Li, W. Li, and R. Tao, "Staged detection–identification framework for cell nuclei in histopathology images," *IEEE Transactions on Instrumentation and Measurement*, vol. 69, no. 1, pp. 183–193, 2019.
- [7] C. Chen, C. Chen, M. Ma, X. Ma, X. Lv, X. Dong, Z. Yan, M. Zhu, and J. Chen, "Classification of multi-differentiated liver cancer pathology images based on deep learning attention mechanism," *BMC Med Inform Decis Mak*, vol. 22, p. 176, July 2022.
- [8] S. S. Raab, D. M. Grzybicki, J. E. Janosky, R. J. Zarbo, F. A. Meier, C. Jensen, and S. J. Geyer, "Clinical impact and frequency of anatomic pathology errors in cancer diagnoses," *Cancer*, vol. 104, pp. 2205–2213, Nov. 2005.
- [9] J. G. Elmore, G. M. Longton, P. A. Carney, B. M. Geller, T. Onega, A. N. A. Tosteson, H. D. Nelson, M. S. Pepe, K. H. Allison, S. J. Schnitt, F. P. O'Malley, and D. L. Weaver, "Diagnostic concordance among pathologists interpreting breast biopsy specimens," *JAMA*, vol. 313, pp. 1122–1132, Mar. 2015.
- [10] R. E. Nakhleh, "Error reduction in surgical pathology," *Arch Pathol Lab*

- Med*, vol. 130, pp. 630–632, May 2006.
- [11] H. Greenspan *et al.*, “Guest editorial deep learning in medical imaging: Overview and future promise of an exciting new technique,” *IEEE Transactions on Medical Imaging*, vol. 35, no. 5, pp. 1153–1159, 2016.
- [12] C. Sun, A. Xu, D. Liu, Z. Xiong, F. Zhao, and W. Ding, “Deep learning-based classification of liver cancer histopathology images using only global labels,” *IEEE J. Biomed. Health Inform.*, vol. 24, no. 6, pp. 1643–1651, 2019.
- [13] M. Chen, B. Zhang, W. Topatana, J. Cao, H. Zhu, S. Juengpanich, Q. Mao, H. Yu, and X. Cai, “Classification and mutation prediction based on histopathology h&e images in liver cancer using deep learning,” *npj Precision Oncology*, vol. 4, p. 14, Jun 2020.
- [14] C. Cortes and V. Vapnik, “Support-vector networks,” *Machine learning*, vol. 20, no. 3, pp. 273–297, 1995.
- [15] A. Krizhevsky, I. Sutskever, and G. E. Hinton, “Imagenet classification with deep convolutional neural networks,” vol. 60, pp. 84–90, AcM New York, NY, USA, 2017.
- [16] K. Simonyan and A. Zisserman, “Very deep convolutional networks for large-scale image recognition,” 2015.
- [17] K. He, X. Zhang, S. Ren, and J. Sun, “Deep residual learning for image recognition,” in *Proceedings of the IEEE Conference on Computer Vision and Pattern Recognition*, pp. 770–778, 2016.
- [18] G. Huang, Z. Liu, L. van der Maaten, and K. Q. Weinberger, “Densely connected convolutional networks,” in *Proceedings of the IEEE Conference on Computer Vision and Pattern Recognition (CVPR)*, pp. 4700–4708, 2017.
- [19] M. Tan and Q. Le, “EfficientNet: Rethinking model scaling for convolutional neural networks,” in *Proceedings of the 36th International Conference on Machine Learning*, pp. 6105–6114, 2019.
- [20] M. Toğaçar, K. B. Özkurt, B. Ergen, and Z. Cömert, “BreastNet: A novel convolutional neural network model through histopathological images for the diagnosis of breast cancer,” *Physica A*, vol. 545, p. 123592, 2020.
- [21] M. Liu *et al.*, “A deep learning method for breast cancer classification in the pathology images,” *IEEE Journal of Biomedical and Health Informatics*, vol. 26, no. 10, pp. 5025–5032, 2022.
- [22] N. O’Mahony, S. Campbell, A. Carvalho, S. Harapanahalli, G. V. Hernandez, L. Krpalkova, D. Riordan, and J. Walsh, “Deep learning vs. traditional computer vision,” pp. 128–144, 2020.
- [23] G. Chakraborty *et al.*, “Grading of hcc biopsy images using nucleus and texture features,” *IEEE Journal of Biomedical and Health Informatics*, vol. 27, no. 1, pp. 65–74, 2023.
- [24] J. Luo, P. Huang, P. He, B. Wei, X. Guo, H. Xiao, Y. Sun, S. Tian, M. Zhou, and P. Feng, “Dca-daffnet: An end-to-end network with deformable fusion attention and deep adaptive feature fusion for laryngeal tumor grading from histopathology images,” *IEEE Transactions on Instrumentation and Measurement*, vol. 72, pp. 1–15, 2023.
- [25] I. Kandel and M. Castelli, “How deeply to fine-tune a convolutional neural network: A case study using a histopathology dataset,” *Appl. Sci.*, vol. 10, no. 10, pp. 1–20, 2020.
- [26] Shallu and R. Mehra, “Breast cancer histology images classification: Training from scratch or transfer learning?,” *ICT Express*, vol. 4, no. 4, pp. 247–254, 2018.
- [27] C. T. Sari *et al.*, “Unsupervised feature extraction via deep learning for histopathological classification of colon tissue images,” *IEEE Transactions on Medical Imaging*, vol. 38, no. 5, pp. 1139–1149, 2018.
- [28] M. Hussain, J. J. Bird, and D. R. Faria, “A study on cnn transfer learning for image classification,” in *UK Workshop on Computational Intelligence*, pp. 191–202, Springer, 2018.
- [29] M. Talo, “Automated classification of histopathology images using transfer learning,” *Artif. Intell. Med.*, vol. 101, no. 101743, pp. 1–10, 2019.
- [30] M. Talo, U. B. Baloglu, Ö. Yıldırım, and U. Rajendra Acharya, “Application of deep transfer learning for automated brain abnormality classification using MR images,” *Cogn. Syst. Res.*, vol. 54, pp. 176–188, May 2019.
- [31] Y. Jin, X. Ye, N. Feng, Z. Wang, X. Hei, J. Liu, L. Mu, and Y. Li, “Lesion classification of coronary artery cta images based on cbam and transfer learning,” *IEEE Transactions on Instrumentation and Measurement*, vol. 73, pp. 1–14, 2024.
- [32] J. Yosinski, J. Clune, Y. Bengio, and H. Lipson, “How transferable are features in deep neural networks?,” *Advances in neural information processing systems*, vol. 27, 2014.
- [33] N. Sarhan, M. Lauri, and S. Frintrop, “Multi-phase fine-tuning: A new fine-tuning approach for sign language recognition,” *KI - Künstliche Intelligenz*, vol. 36, pp. 91–98, Mar 2022.
- [34] N. Tajbakhsh *et al.*, “Convolutional neural networks for medical image analysis: Full training or fine tuning?,” *IEEE Transactions on Medical Imaging*, vol. 35, no. 5, pp. 1299–1312, 2016.
- [35] M. Macenko, M. Niethammer, J. S. Marron, D. Borland, J. T. Woosley, X. Guan, C. Schmitt, and N. E. Thomas, “A method for normalizing histology slides for quantitative analysis,” in *IEEE International Symposium on Biomedical Imaging: From Nano to Macro*, pp. 1107–1110, 2009.
- [36] A. A. Borkowski, M. M. Bui, L. B. Thomas, C. P. Wilson, L. A. DeLand, and S. M. Mastorides, “Lung and colon cancer histopathological image dataset (lc25000),” 2019.
- [37] A. Paszke, S. Gross, F. Massa, A. Lerer, J. Bradbury, G. Chanan, T. Killeen, Z. Lin, N. Gimelshein, L. Antiga, A. Desmaison, A. Kopf, E. Yang, Z. DeVito, M. Raison, A. Tejani, S. Chilamkurthy, B. Steiner, L. Fang, J. Bai, and S. Chintala, “Pytorch: An imperative style, high-performance deep learning library,” in *Advances in Neural Information Processing Systems*, pp. 8024–8035, Curran Associates, Inc., 2019.
- [38] I. Loshchilov and F. Hutter, “Sgdr: Stochastic gradient descent with warm restarts,” 2017.
- [39] L. Xia, Z. Qu, J. An, and Z. Gao, “A weakly supervised method with colorization for nuclei segmentation using point annotations,” *IEEE Transactions on Instrumentation and Measurement*, vol. 72, pp. 1–11, 2023.
- [40] A. Mencattini, M. Salmeri, G. Rabottino, and S. Salicone, “Metrological characterization of a cadx system for the classification of breast masses in mammograms,” *IEEE Transactions on Instrumentation and Measurement*, vol. 59, no. 11, pp. 2792–2799, 2010.
- [41] F. A. Spanhol, L. S. Oliveira, C. Petitjean, and L. Heutte, “A dataset for breast cancer histopathological image classification,” *IEEE Transactions on Biomedical Engineering*, vol. 63, no. 7, pp. 1455–1462, 2016.